Electronic Supplementary Material (ESI) for RSC Advances.

The stability of $CsPb(Br_xCl_{1-x})_3$ All-Inorganic Mix-halide Perovskite

Chun-Wei Zhu, Xiao-Tong Yan, Yu-Jun Zhao, Xiao-Bao Yang*

Department of Physics, South China University of Technology, Guangzhou 510640, PR China

Supplementary Materials

* Corresponding author.

E-mail: scxbyang@scut.edu.cn (X.-B. Yang).

Table S1 The inorganic perovskite crystal system type at different synthesis methods

Year	Material	Type	Synthesis method	Crystal system	Ref
2022	$CsPbBr_xCl_{3-x}$	nanocomposite films	Solution method	Cubic	[1]
2023	$CsPbBr_{1.8}Cl_{1.2}$	Thin films	Solution method	Orthorhombic	[2]
2022	$CsPbBr_xCl_{3-x}$	Nanocrystals	Hot-injection	Cubic	[3]
2020	$CsPbBr_3$	QDs	hot-injection	Cubic	[4]
2016	$CsPbBr_xCl_{3-x}$	QDs	Room temperature	Cubic/Monoclinic	[5]
2016	$CsPbBr_xCl_{3-x}$	QDs	Hot-injection	Cubic	[5]
2022	$CsPb(Br_{1-x}Cl_x)_3$	Polycrystalline thin film	Thermal evaporation approach	Orthorhombic	[6]
2013	$CsPbBr_3$	Single crystal	Bridgman method	Orthorhombic	[7]
2021	$CsPbBr_{3-x}Cl_x$	3D	Solution method	Orthorhombic	[8]
2018	$CsPbBr_3$	Single crystal	Bridgman-Stockbarger	Tetragonal	[9]
2015	$CsPbBr_3$	Nanowires/single crystals	Solution-phase synthesis	Orthorhombic	[10]
2015	$CsPbBr_3$	Nanoplates/Anisotropic	Hot-injection	Cubic	[11]
2016	$CsPbBr_{3-x}Cl_x/CsPbBr_{3-x}I_x$	Nanowires	Solution-phase synthesis	Orthorhombic	[12]
2016	$CsPbBr_3$	Nanowires	Hot-injection	Orthorhombic/Cubic	[13]
2017	$CsPbBr_3$	Nanowires	CVD	Monoclinic	[14]
2017	$CsPbBr_3$	Nanowires	Ultrasonication	Orthorhombic	[15]
2019	$CsPbBr_3$	Nanowires	VLS	Cubic	[16]
2017	$CsPbCl_3$	Quantum dot	Hot-injection	Cubic	[17]
2018	$CsPbCl_3$	Nanocrystals	Hot-injection	Cubic	[18]

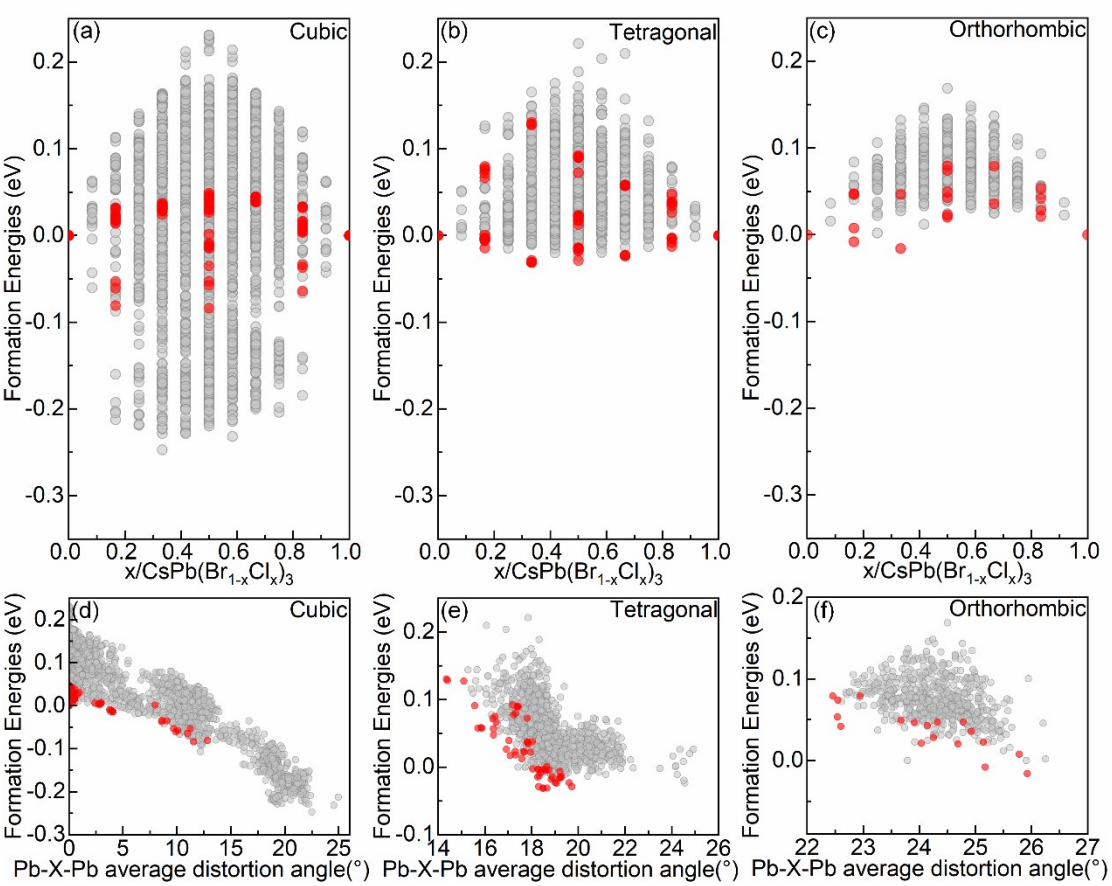

Figure S1 The relative stability of ordered configurations among the three alloy systems (a) Cubic (b)Tetragonal (c) Orthorhombic alloy system and the relative positions in the Pb-X-Pb (X=Br/Cl) average distortion angle dimension of above configurations for (d) Cubic (e) Tetragonal (f) Orthorhombic alloy system.

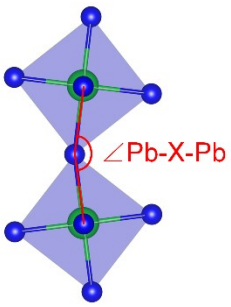

Figure S2 The schematic illustration of ∠Pb-X-Pb (X=Br or X=Cl)

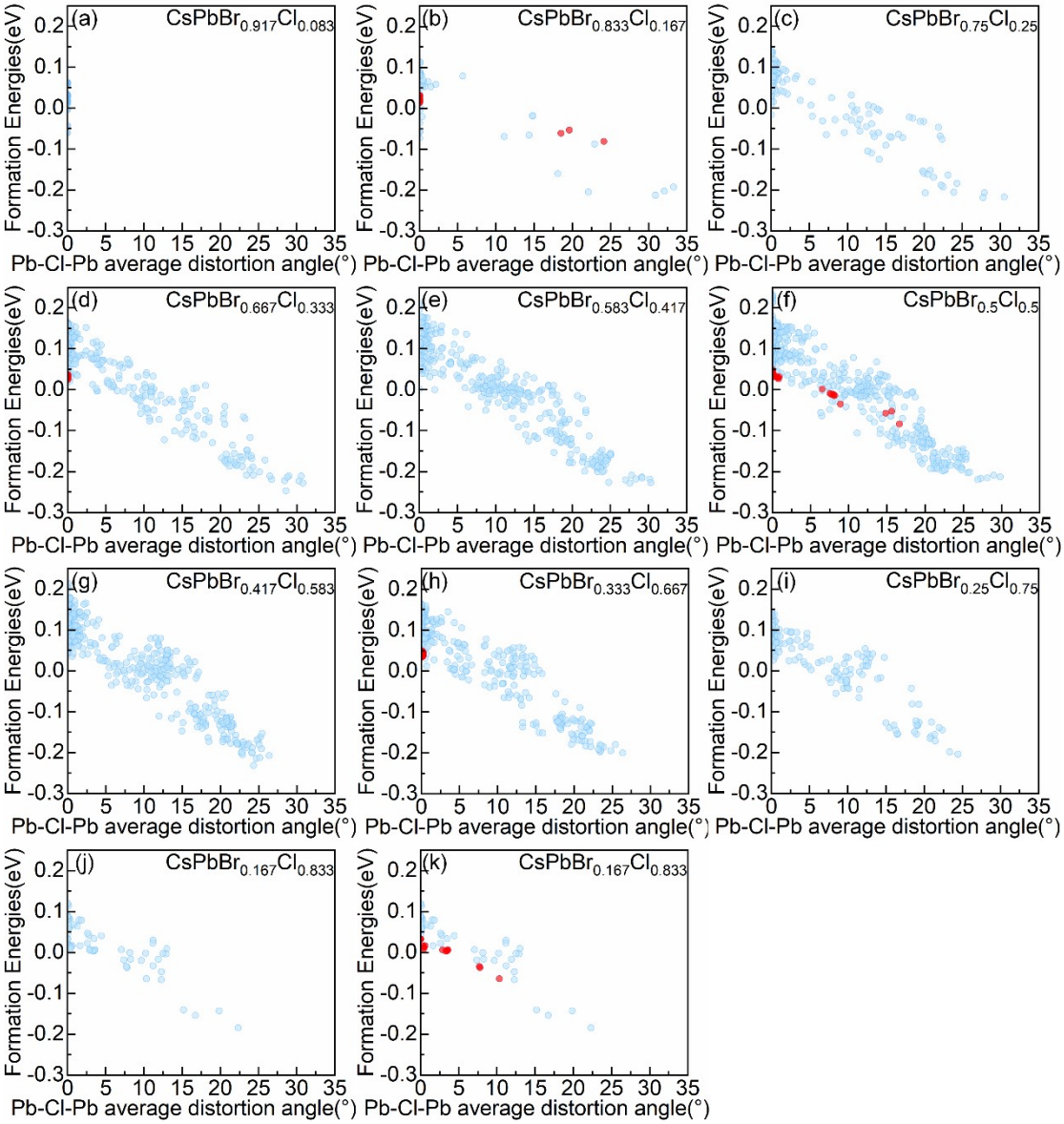

Figure S3 Relationship between formation energies of symmetry-nonequivalent configurations and the Pb-Cl-Pb average distortion angle in the cubic alloy system at various concentrations. Red dots represent ordered configuration.

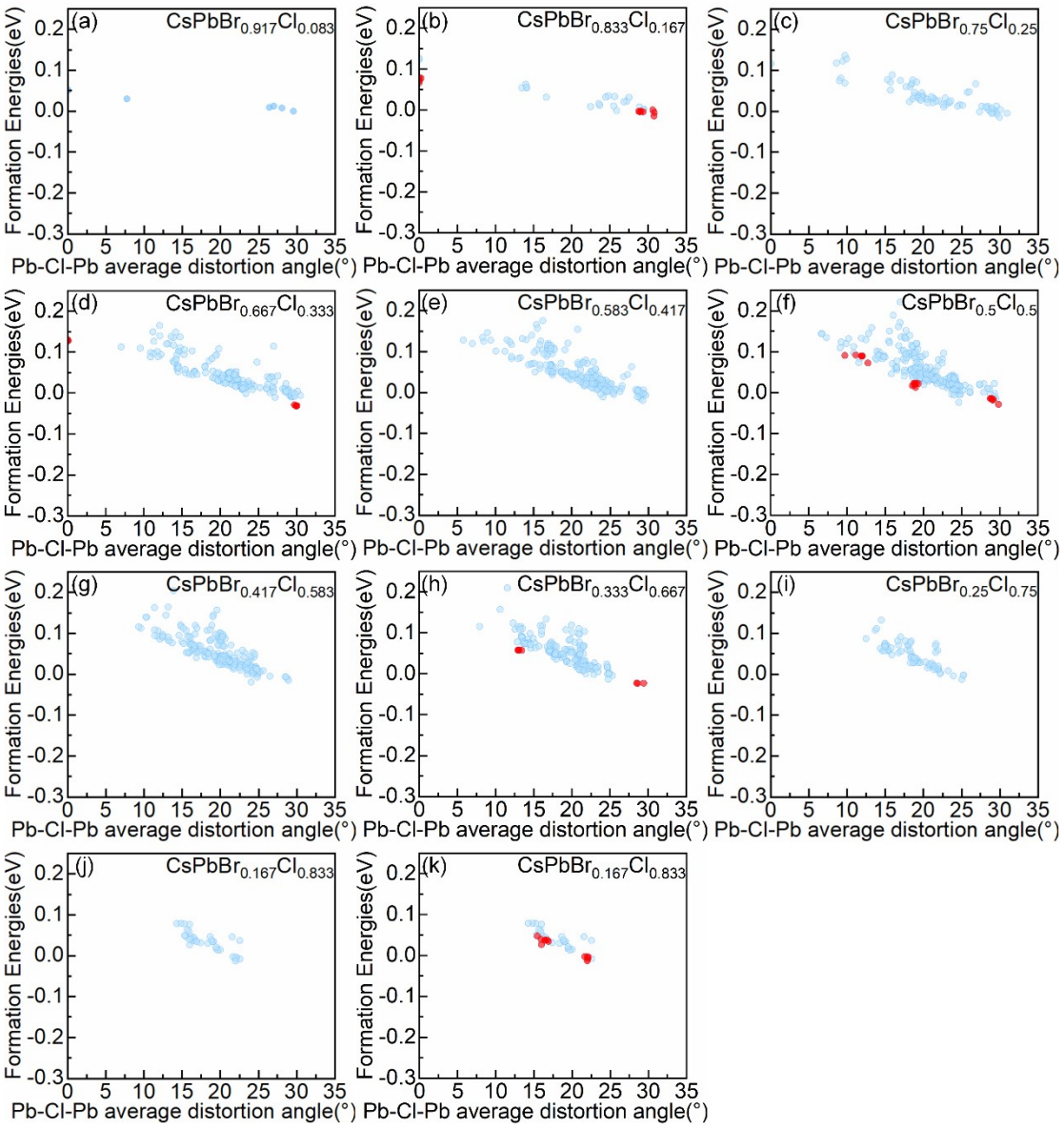

Figure S4 Relationship between formation energies of symmetry-nonequivalent configurations and the Pb-Cl-Pb average distortion angle in the tetragonal alloy system at various concentrations. Red dots represent ordered configuration.

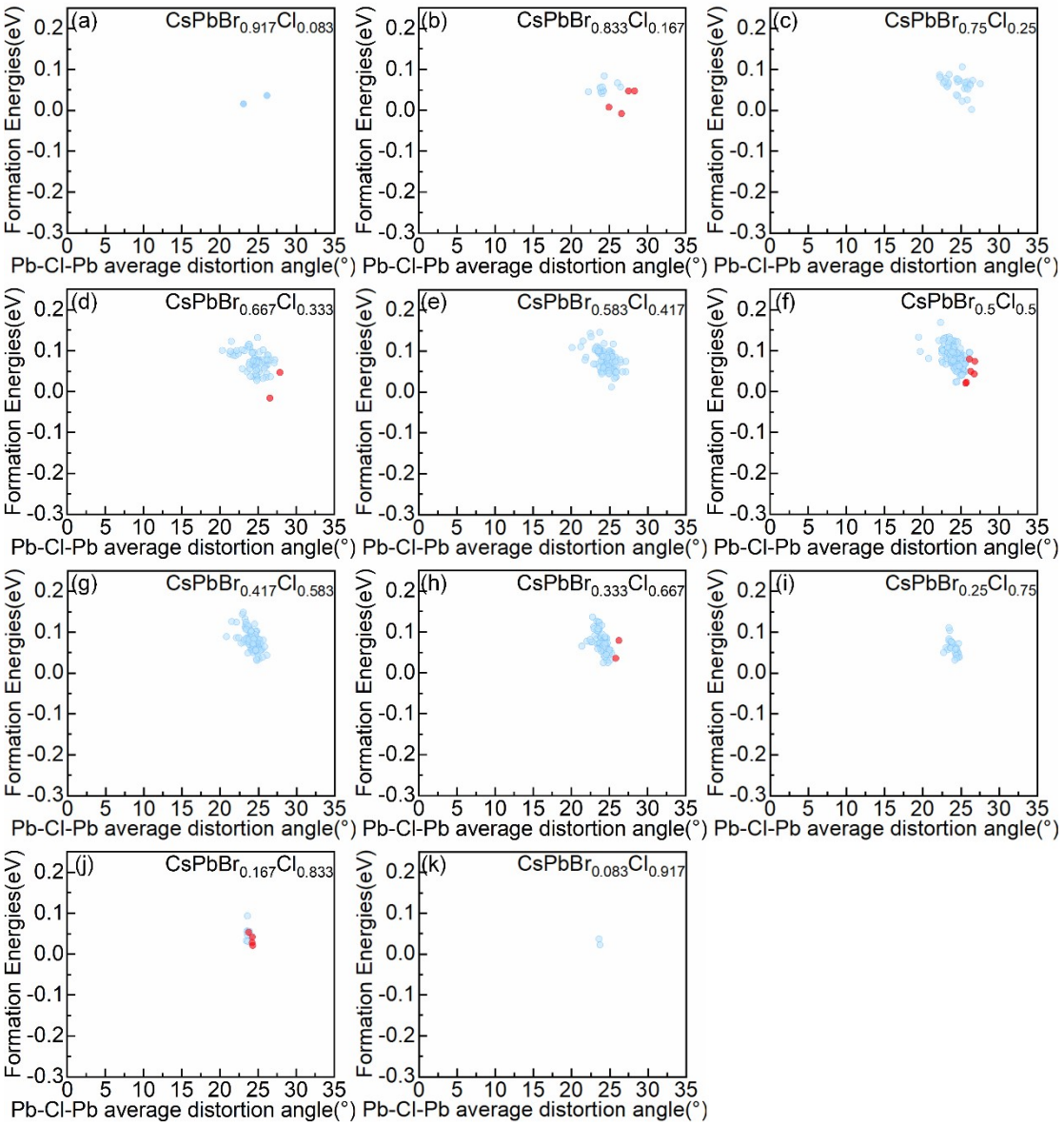

Figure S5 Relationship between formation energies of symmetry-nonequivalent configurations and the Pb-Cl-Pb average distortion angle in the orthorhombic alloy system at various concentrations. Red dots represent ordered configuration.

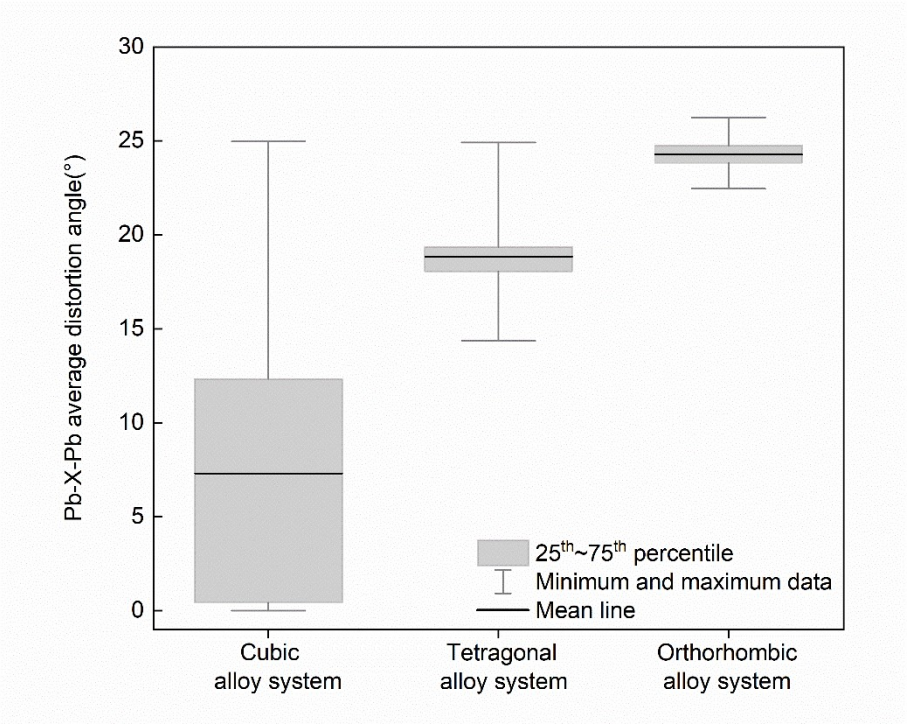

Figure S6 Shows the distribution ranges of the Pb-X-Pb (X=Br/Cl) average distortion angle in the orthorhombic, tetragonal, and cubic alloy systems.

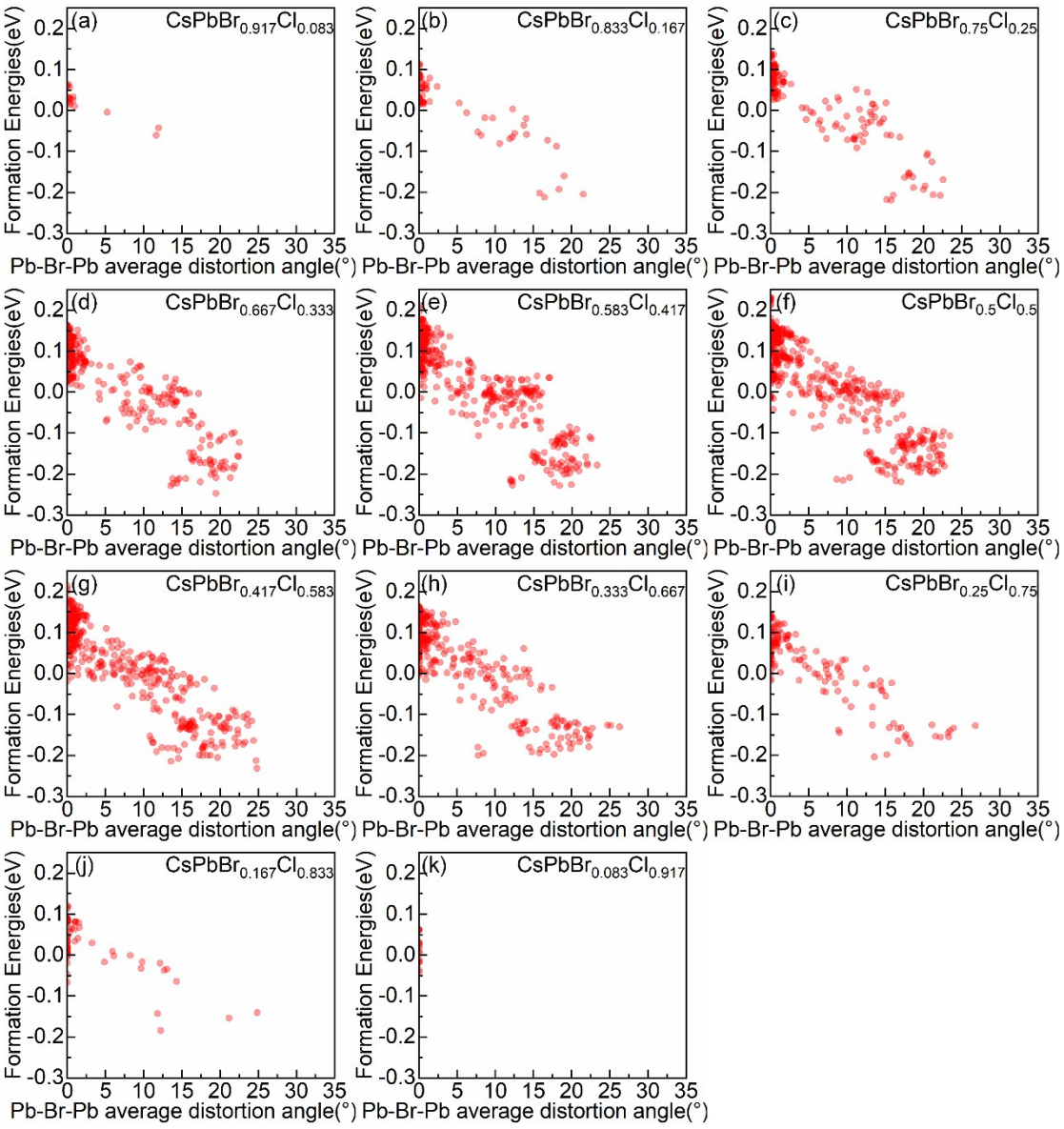

Figure S7 Relationship between formation energies of symmetry-nonequivalent configurations and the Pb-Br-Pb average distortion angle in the cubic alloy system at various concentrations.

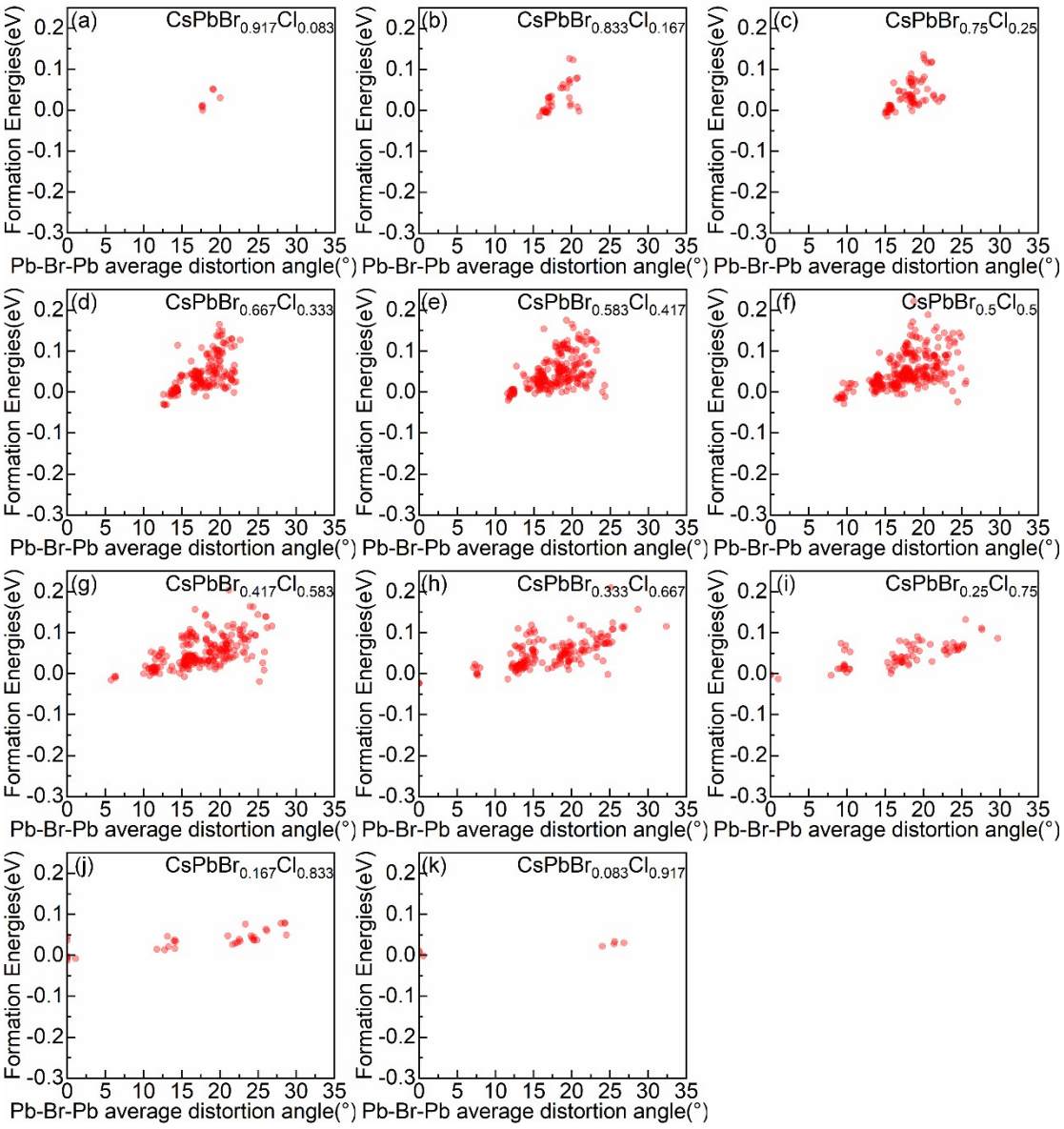

Figure S8 Relationship between formation energies of symmetry-nonequivalent configurations and the Pb-Br-Pb average distortion angle in the tetragonal alloy system at various concentrations.

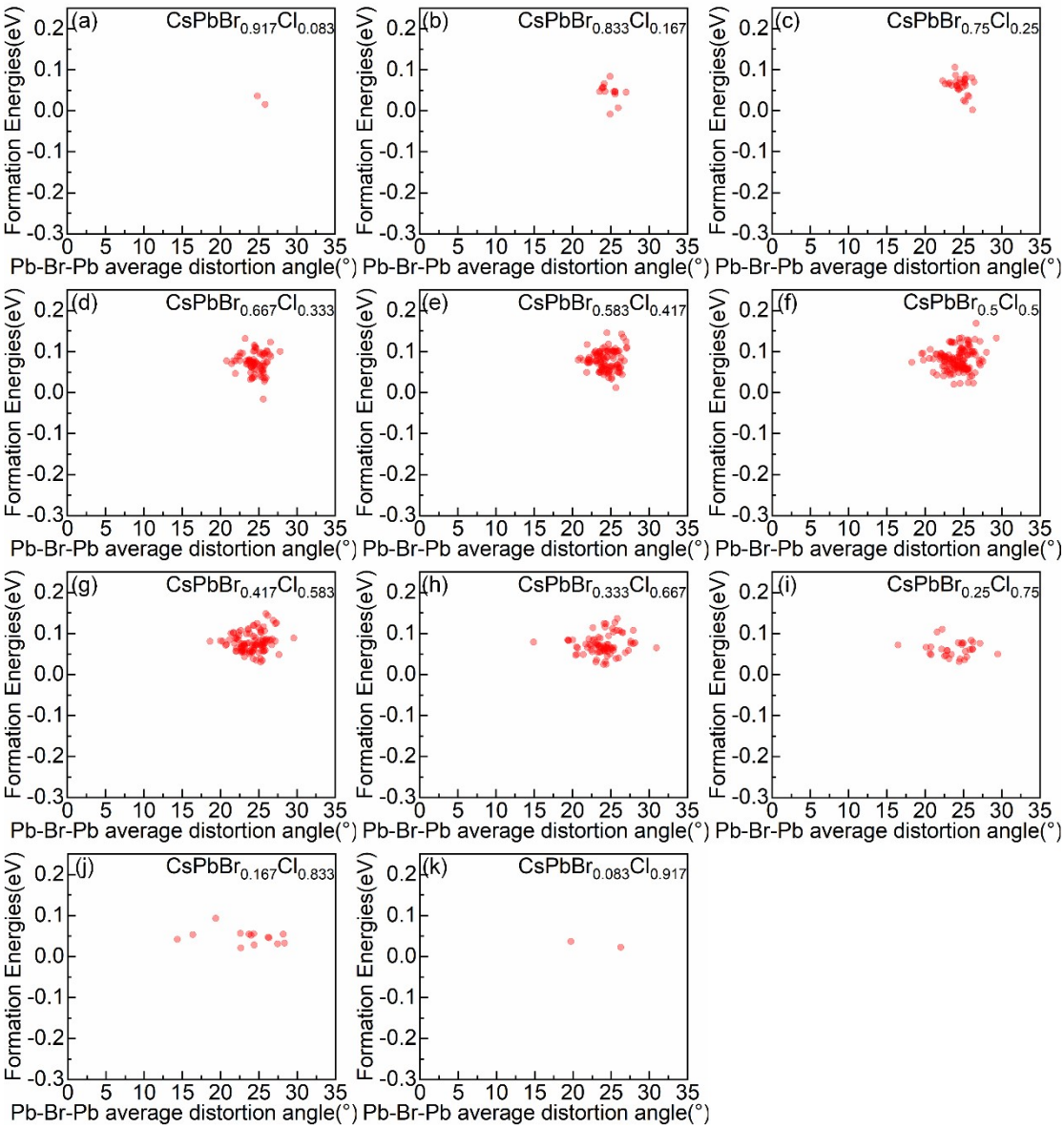

Figure S9 Relationship between formation energies of symmetry-nonequivalent configurations and the Pb-Br-Pb average distortion angle in the orthorhombic alloy system at various concentrations.

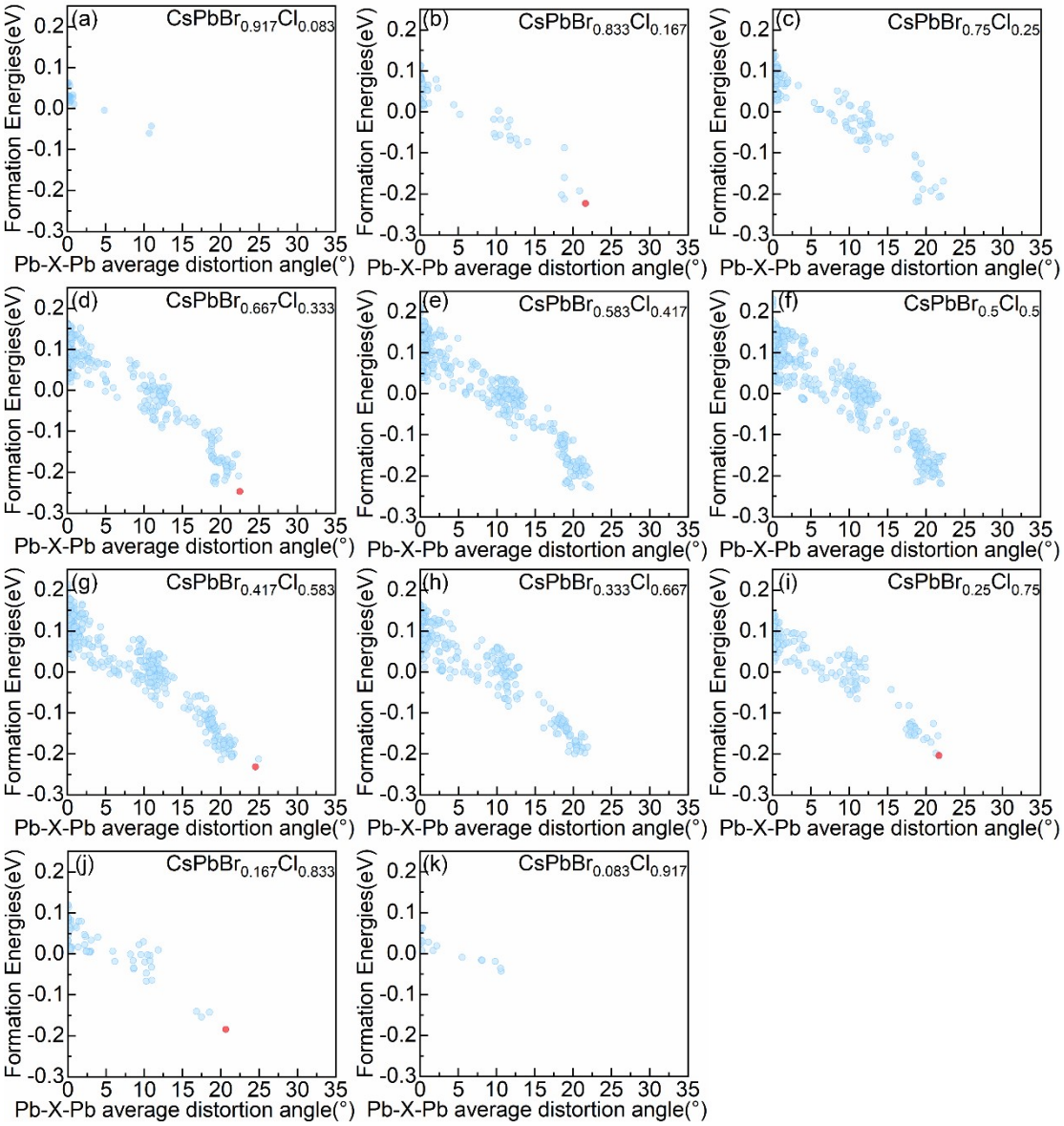

Figure S10 Relationship between formation energies of symmetry-nonequivalent configurations and the Pb-X-Pb (X=Br/Cl) average distortion angle in the cubic alloy system at various concentrations. Red dots represent convex point configuration.

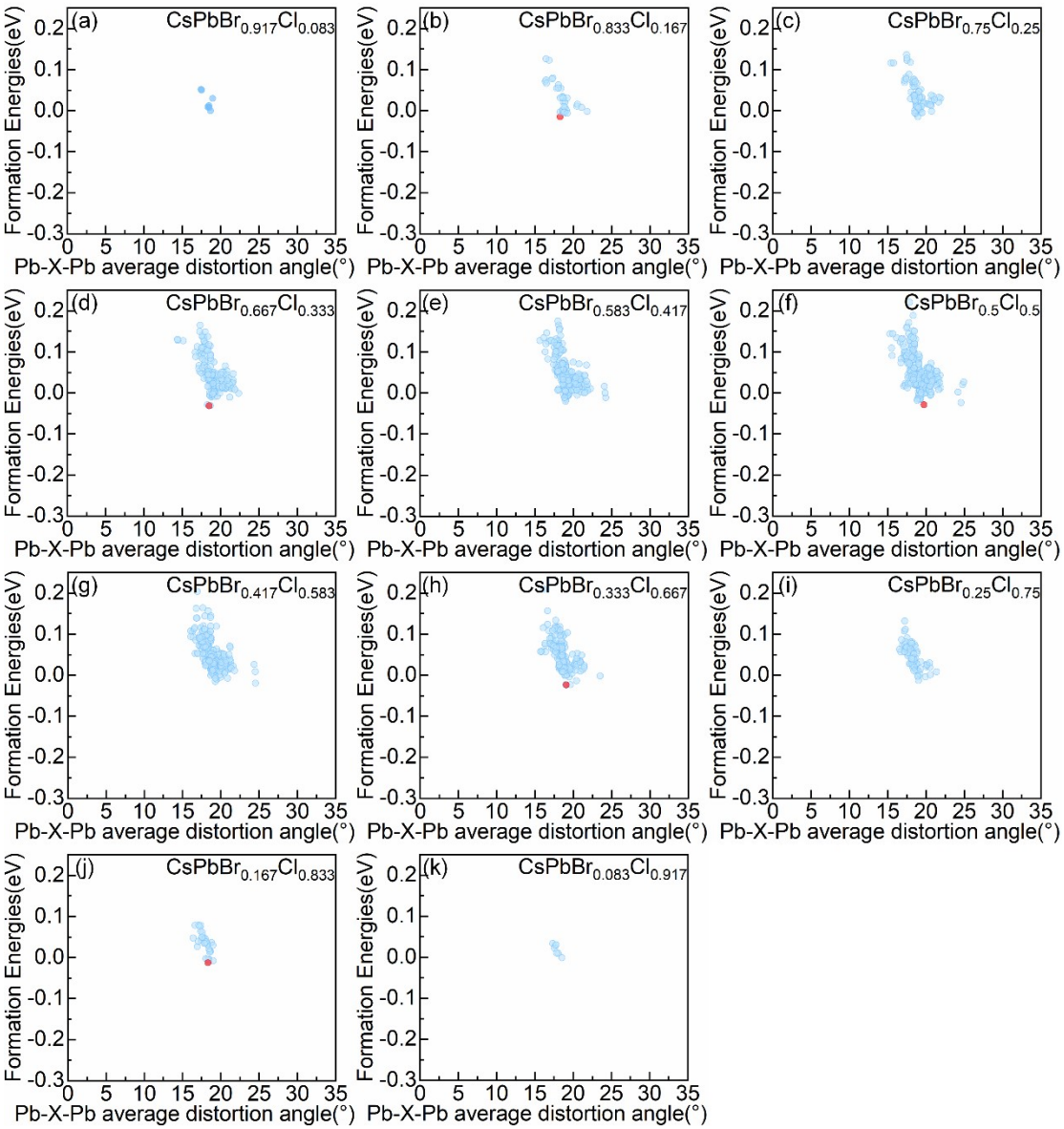

Figure S11 Relationship between formation energies of symmetry-nonequivalent configurations and the Pb-X-Pb (X=Br/Cl) average distortion angle in the tetragonal alloy system at various concentrations. Red dots represent convex point configuration.

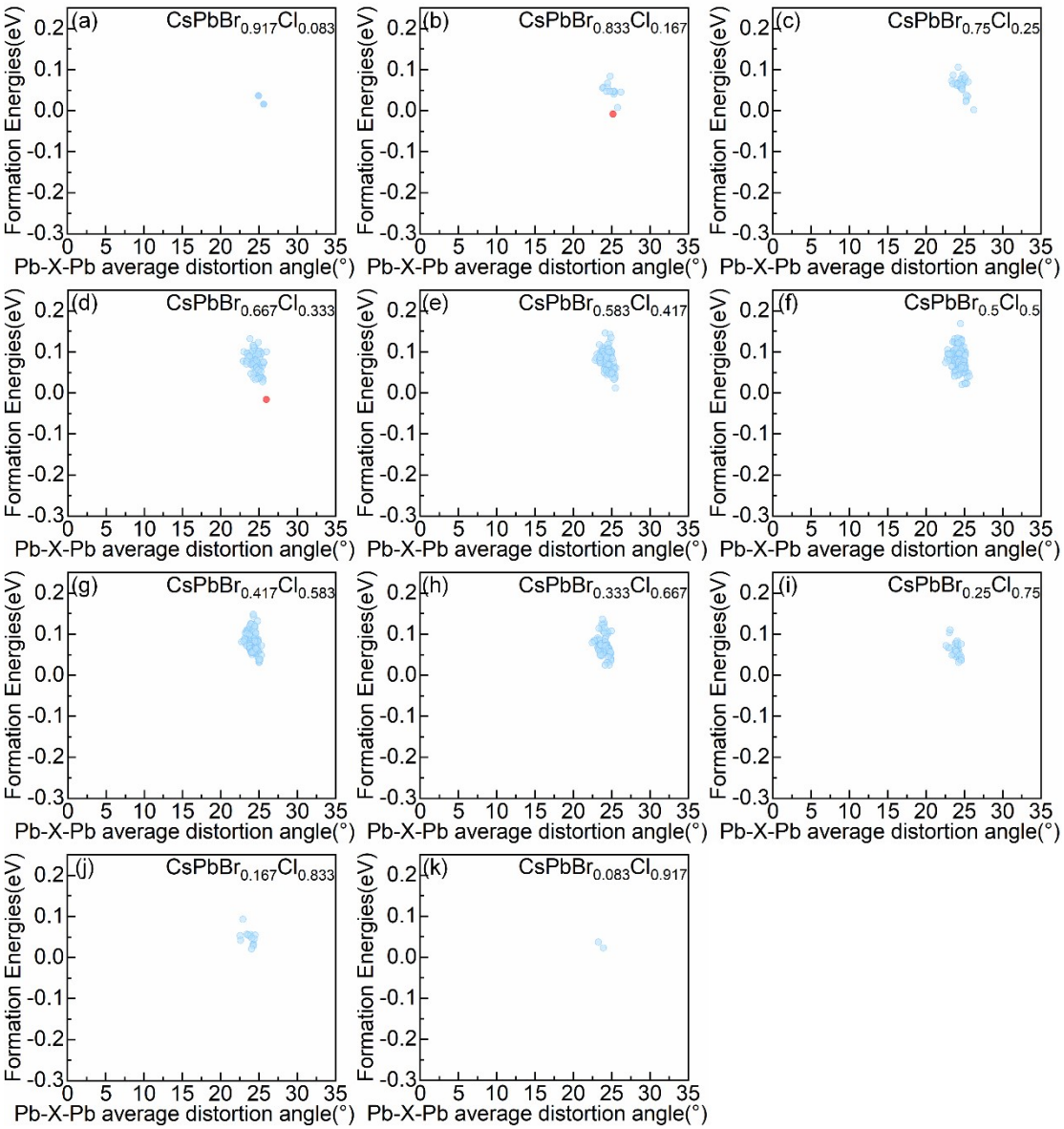

Figure S12 Relationship between formation energies of symmetry-nonequivalent configurations and the Pb-X-Pb (X=Br/Cl) average distortion angle in the orthorhombic alloy system at various concentrations. Red dots represent convex point configuration.

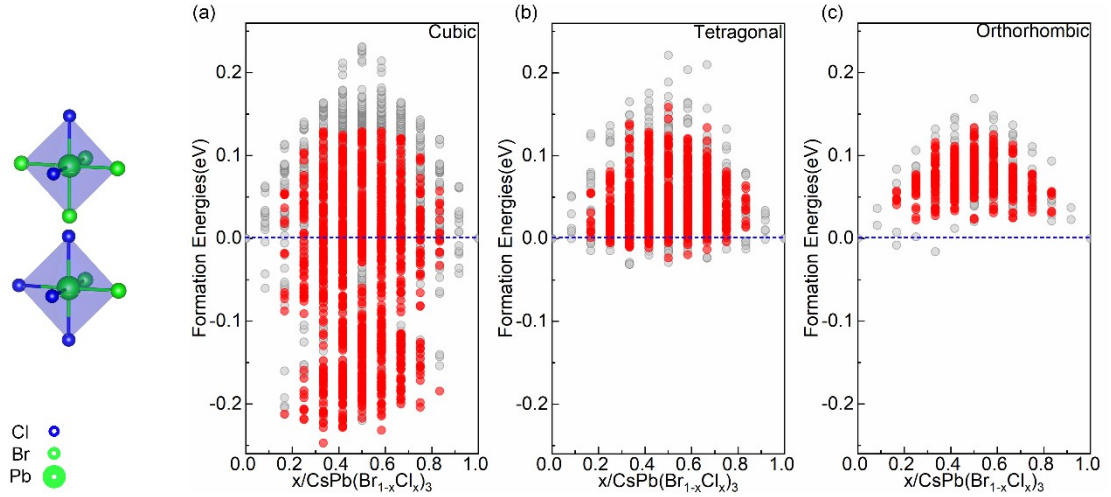

Figure S13 The relative positions in the convex hull diagram of configurations containing the left side two low symmetric octahedra of the three alloy systems (a) cubic (b) tetragonal (c) orthorhombic alloy systems.

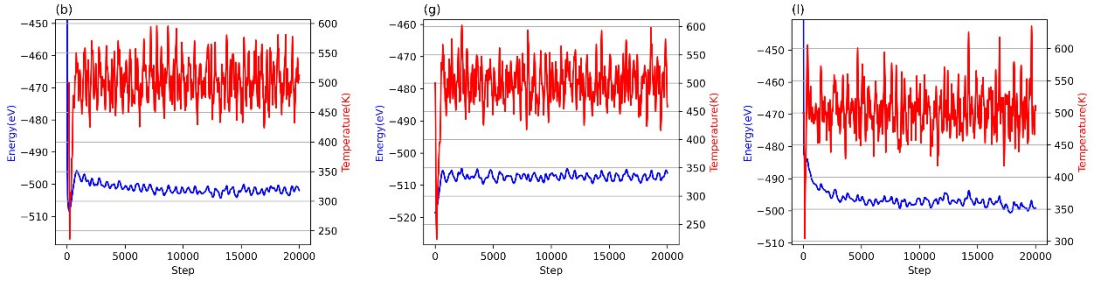

Figure S14 Molecular simulations at an equilibrium temperature of 500 K for cubic convex point configurations (b), tetragonal convex point configurations (g) and orthorhombic convex point configuration (l).

References

1 I. Y. Choi, S. Baek, A. V. Takaloo, S. Y. Lee, A. Hajibabaei, K. S. Kim and J. Myoung, *Adv. Opt. Mater.*, 2022, **10**, 2102502.

2 R. R. Sumukam, G. S. Kumar, R. N. Savu and B. Murali, *J. Phys. Chem. Lett.*, 2023, **14**, 395–402.

3 S. Yuan, X. Zheng, W.-S. Shen, J. Liu, L.-S. Cui, C. Zhang, Q.-S. Tian, J.-J. Wu, Y.-H. Zhou, X.-D. Wang, Z.-K. Wang, P. Han, J. M. Luther, O. M. Bakr and L.-S. Liao, *ACS Energy Lett.*,

2022, **7**, 1348–1354.

4 S. Shi, Y. Wang, S. Zeng, Y. Cui and Y. Xiao, *Adv. Opt. Mater.*, 2020, **8**, 2000167.

5 X. Li, Y. Wu, S. Zhang, B. Cai, Y. Gu, J. Song and H. Zeng, *Adv. Funct. Mater.*, 2016, **26**, 2435–2445.

6 Y. Li, Q. Liu, X. Liu, J. Feng, L. He, H. Li, C. Li and H. Zhang, *J. Phys. Chem. Lett.*, 2021, **12**, 10746–10752.

7 C. C. Stoumpos, C. D. Malliakas, J. A. Peters, Z. Liu, M. Sebastian, J. Im, T. C. Chasapis, A. C. Wibowo, D. Y. Chung, A. J. Freeman, B. W. Wessels and M. G. Kanatzidis, *Cryst. Growth Des.*, 2013, **13**, 2722–2727.

8 W. Ding, H. Liu, S. Zhang, D. Qiu, X. Li and S. Wang, *Adv. Funct. Mater.*, 2022, **32**, 2105164.

9 R. Dos Reis, H. Yang, C. Ophus, P. Ercius, G. Bizarri, D. Perrodin, T. Shalapska, E. Bourret, J. Ciston and U. Dahmen, *Appl. Phys. Lett.*, 2018, **112**, 071901.

10 D. Zhang, S. W. Eaton, Y. Yu, L. Dou and P. Yang, *J. Am. Chem. Soc.*, 2015, **137**, 9230–9233.

11 Y. Bekenstein, B. A. Koscher, S. W. Eaton, P. Yang and A. P. Alivisatos, *J. Am. Chem. Soc.*, 2015, **137**, 16008–16011.

12 D. Zhang, Y. Yang, Y. Bekenstein, Y. Yu, N. A. Gibson, A. B. Wong, S. W. Eaton, N. Kornienko, Q. Kong, M. Lai, A. P. Alivisatos, S. R. Leone and P. Yang, *J. Am. Chem. Soc.*, 2016, **138**, 7236–7239.

13 D. Zhang, Y. Yu, Y. Bekenstein, A. B. Wong, A. P. Alivisatos and P. Yang, *J. Am. Chem. Soc.*, 2016, **138**, 13155–13158.

14 M. Shoaib, X. Zhang, X. Wang, H. Zhou, T. Xu, X. Wang, X. Hu, H. Liu, X. Fan, W. Zheng, T. Yang, S. Yang, Q. Zhang, X. Zhu, L. Sun and A. Pan, *J. Am. Chem. Soc.*, 2017, **139**, 15592–

15595.

15 Y. Tong, B. J. Bohn, E. Bladt, K. Wang, P. Müller-Buschbaum, S. Bals, A. S. Urban, L. Polavarapu and J. Feldmann, *Angew. Chem. - Int. Ed.*, 2017, **56**, 13887–13892.

16 Y. Meng, C. Lan, F. Li, S. Yip, R. Wei, X. Kang, X. Bu, R. Dong, H. Zhang and J. C. Ho, *ACS Nano*, 2019, **13**, 6060–6070.

17 J. Zhang, Q. Wang, X. Zhang, J. Jiang, Z. Gao, Z. Jin and S. (Frank) Liu, *RSC Adv.*, 2017, **7**, 36722–36727.

18 Z.-J. Yong, S.-Q. Guo, J.-P. Ma, J.-Y. Zhang, Z.-Y. Li, Y.-M. Chen, B.-B. Zhang, Y. Zhou, J. Shu, J.-L. Gu, L.-R. Zheng, O. M. Bakr and H.-T. Sun, *J. Am. Chem. Soc.*, 2018, **140**, 9942–9951.